

MET.O.14

METEOROLOGICAL OFFICE
BOUNDARY LAYER RESEARCH BRANCH
TURBULENCE & DIFFUSION NOTE



T.D.N. No. 101

ON THE INTERACTION OF TOPOGRAPHY AND EKMAN
BOUNDARY LAYER PUMPING IN A STRATIFIED ATMOSPHERE

by

P.J.Mason & R.I.Sykes

June 1977

Please note: Permission to quote from this unpublished note should be
obtained from the Head of Met.O.14, Bracknell, Berks, U.K.

FH10

Original typescript

77/71

On the interaction of topography and Ekman boundary
layer pumping in a stratified atmosphere

P.J. Mason

and R.I. Sykes

Meteorological Office, Bracknell
(Received 27 June 1977)

(Received 27 June 1977)

SUMMARY

A simple theory of the interaction of topography and Ekman boundary layer pumping in a stratified atmosphere is presented together with numerical solutions of the corresponding two-dimensional NavierStokes equation problem. Numerical results for flow over a two-dimensional ridge confirm theoretical predictions that stratification enhances the momentum coupling and produces a low-level jet parallel to the ridge.

1. Introduction

In meteorology a detailed knowledge of flow over topography is required in a number of contexts. The flow field may be required in relation to problems in local forecasting and pollutant dispersal whilst certain gross characteristics are needed to facilitate parameterisation of sub-grid scales of topography in general circulation and forecasting models. At present understanding of these flows is very limited and the present work seeks to elucidate some important effects which occur on length scales of the order of hundreds of kilometres.

When considering the momentum coupling of the atmosphere to the Earth it is convenient to distinguish between the synoptic scale pressure forces acting on mountains and the drag due to the turbulent boundary layer. Owing to the lack of smooth surfaces on our planet the latter drag is of course itself mainly the result of pressure forces acting on sub-synoptic scales. Direct measurements of the drag due to turbulent boundary layers are generally on scales which take account of vegetation and very small hills but the inclusion of larger scales is a matter of great uncertainty. With regard to topography with horizontal lengths of the order of hundreds of kilometres we can present order of magnitude arguments, substantiated by the numerical results of § 4, regarding the importance of various mechanisms.

In a neutral atmosphere the aerodynamic pressure drag on a hill of height h and characteristic horizontal length L would be expected to be $\sim C_h \frac{1}{2} \rho U^2 L h$ (Batchelor 1967) where U is the typical flow speed ρ the fluid density and C_h a drag coefficient generally expected to be somewhat less than unity. The magnitude of the force due to the turbulent boundary layer stress on this length scale L will be $\sim C_g \rho U_g^2 L^2$ where U_g is the geostrophic wind and C_g the so-called geostrophic drag coefficient having a typical value $\sim 2 \cdot 10^{-3}$ (Smith 1975). If we assume $C_h \sim 0.1$ it follows that aerodynamic pressure drag might be expected to be

important when $h/L \gtrsim 20$ but for the length scales $L \gtrsim 100$ km and $h \sim 1$ km considered in this paper it should be negligible.

In a stably stratified atmosphere a pressure force due to the radiation of internal gravity waves away from the topography would be expected. Such an effect cannot be parameterised in terms of a boundary layer drag since the flow retardation occurs where the wave motion is dissipated, usually remote from the boundary layer. There is a substantial literature on this subject but for the present purposes we simply consider an order of magnitude argument consistent with the linearised theory given by Queney (1947).

For simplicity we will assume the Brunt Vaisala frequency $N = \left(\frac{g}{\bar{\rho}} \frac{\partial \rho_0}{\partial z} \right)^{1/2} \sim 10^{-2} \text{ s}^{-1}$ being a typical atmospheric value where g is the acceleration due to gravity, $\bar{\rho}$ the mean density, $\frac{\partial \rho_0}{\partial z}$ the undisturbed vertical density gradient) to be independent of height, so the governing dispersion relation is (Bretherton 1969)

$$(\omega - U_g k)^2 = \frac{N^2 (k^2 + l^2)}{(m^2 + k^2 + l^2)}$$

where ω is the wave frequency, m the vertical wavenumber and k and l the horizontal wavenumbers. For circumstances under which the Froude number

$U_g / N L > 1$ little gravity wave drag can occur as the main disturbances are evanescent. For smaller values of Froude number gravity wave drag is more effective and we consider a disturbance to be produced with vertical velocity w' of typical magnitude $2U_g h/L$. The gravity wave drag arises as a result of energy radiating away from an area L^2 with a group velocity V . For small Froude number it follows from the dispersion relation that $m \sim \frac{N}{U_g}$ and $V \sim \frac{2N U_g}{L N}$. Hence from continuity the magnitude of the horizontal velocity disturbances, $u' = w' m / k$, is much greater than w' . The energy density of the radiating waves E is thus $\frac{1}{2} \bar{\rho} u'^2$ and the magnitude of the gravity wave drag

$$\sim E \cdot L^2 \cdot V / U_g$$

$$\sim \bar{\rho} U_g N h^2 L / \pi$$

It follows that for mountains with $h \sim 10^3 m$ and $L \lesssim 200 km$ gravity wave drag is potentially more important than typical values of the drag due to a turbulent boundary layer. At length scales $\gtrsim 100 km$ effects due to the basic rotation become important and we should consider inertia-gravity waves governed by the dispersion relation (Bretherton 1969)

$$(\omega - u_y k)^2 = \frac{N^2 (k^2 + l^2) + f^2 m^2}{k^2 + l^2 + m^2}$$

where f is the Coriolis parameter. In a neutral atmosphere inertial wave drag can occur and bounds on its magnitude can be estimated in a similar way to the above discussion of gravity wave drag (Mason 1977). In a vertically unbounded neutral atmosphere with $u_y k / f \ll 1$ the drag force is $\sim \bar{g} f u_y L h^2$ and negligible compared with that due to a turbulent boundary layer. In practice, apart from the vertical boundedness of the atmosphere, the effect of an additional stable stratification such that $u_y k / N \ll 1$ is to make the disturbance evanescent.

In the absence of effects depending on baroclinicity it is probable that the only other appropriate class of wave radiation would be that the Rossby waves. Again we may use simple group velocity arguments and assume the topography is sufficiently large to give wave amplitude $\sim U_g$. We then obtain an estimate of the drag as $\sim \bar{g} L^3 u_y \beta / 8 \pi^2$ where $\beta = |\nabla f|$.

Such a drag is only important on the largest planetary scales and in principle is well represented by forecasting and general circulation models.

Baroclinic effects not only alter the vorticity gradients present within the fluid with consequent effects on Rossby wave properties but also admit other forms of wave motion such as neutral (Rhines 1970) and growing baroclinic waves (Eady 1949). Very little is known about the effect of topography in a baroclinic atmosphere but it is reasonable to suppose that the principle effects occur on scales comparable with typical synoptic scale baroclinic eddies.

The mechanism for drag considered in this paper does not involve the radiation of energy but rather viscous dissipation of the standing disturbance produced by the topography, and is thus, in a sense akin to the aerodynamic drag. The dissipation mechanism is the Ekman boundary layer pumping associated with the "spin up" process and is the prime dissipation mechanism on the synoptic and global scales. On the scales we are considering, the role of the atmosphere's basic stratification is crucial. In a neutral atmosphere the dissipation is of little consequence, but stratification restricts the vertical scale of the disturbance and thereby increases both its amplitude and vulnerability to the spin up process.

The drag we obtain would not be given by a coarse resolution numerical model with smoothed topography and in current forecasting and general circulation models forms part of the boundary layer parameterisation problem. With regard to local flow problems the present mechanism gives significant effects including low level jets at the top of the boundary layer.

In § 2 we present a simple linearised theory which has some success in describing the mechanism whilst in § 3 we describe a numerical model used to conduct a fuller investigation. In § 4 the results of the numerical work are given and finally in § 5 the conclusions.

2. Theory

In the two-dimensional numerical model of § 3 and the analytic results obtained in this section we choose to study a problem with periodic boundary conditions in the direction of the basic flow. When the analytic theory is posed as three-dimensional, this choice is not essential, but for two-dimensional problems in a vertically bounded fluid with Rossby number $u_g / fL < 1$ it is vital.

The reason lies in the singularity of the non-periodic two-dimensional problem. This is most clearly demonstrated in the work of Huppert and Stern (1974).

They considered the flow of a fluid of depth D over a small two-dimensional ridge perpendicular to the vertical side walls in a channel rotating about a vertical axis, and compared their results with the corresponding two-dimensional problem. The latter problem of geostrophic flow over a ridge is frequently given in textbooks on meteorology. In passing over the ridge, the flow is permanently deflected, making an angle $\tan^{-1} (fA/DU_0)$ to the original direction, where A is the cross-sectional area of the ridge. In the

three-dimensional problem with side walls, no matter what separation of side walls is taken, the net deflection far downstream is zero and so is the net streamline displacement and the pressure force on the ridge. However, the local flow over the ridge is characterised by the deflection found in the two-dimensional problem. The presence of side walls gives rise to upstream influence on a length scale of the order of the side wall separation.

The two-dimensional solution is thus demonstrated to be singular and the non-physical nature of the solution is further evinced by considering the pressure forces acting on the ridge. In the two-dimensional problem a pressure field consistent with the deflection of the flow gives rise to a drag force on the object. This force is not balanced by viscous dissipation or wave radiation, both of which are zero in the problem posed, but by boundary conditions which must be chosen to fit the solution. The periodic two-dimensional problem does not suffer from these difficulties; the periodicity circumvents the upstream influence and the solution corresponds to the limit obtained with remote side walls.

Previous work in this area has not always recognised this difficulty with two-dimensional problems and part of the work of Merkin (1975) and Janowitz (1975) contains such erroneous solutions. These solutions are of value in describing aspects of the local flow but give spurious values of drag force.

Before presenting the linear theory of the stratified case we will outline some results for a vertically bounded homogeneous fluid.

(a) Homogeneous case

We first consider the problem of homogeneous flow between bounding surfaces distance D apart, illustrated in figure 1. We assume that the Rossby number $R = U_g/fL$ is small. In the absence of topography, an Ekman boundary layer of thickness $\delta = (\nu/\Omega)^{1/2}$, where ν is the kinematic viscosity of the fluid and $\Omega = f/2$, forms on the lower no-slip boundary. We assume the upper boundary is stress-free, implying no boundary layers on the upper surface. Provided the Ekman number $E = \frac{\delta}{D}$ is small, the main part of the fluid is governed by the inviscid equations of motion, and the dynamics will be dominated by rotational effects, since the Rossby number is small. The principal effect is the 'vortex stretching' mechanism, see eg Batchelor (1967). The vertical length scale associated with L in a rapidly rotating fluid is of order L/R , and here we shall assume $D \ll L/R$, so that the interior flow is independent of the vertical coordinate. This is the well-known Taylor-Proudman theorem; the fluid moves in columns, which vary in length as the fluid passes over the topography. This induces vorticity in the interior motion, and is one of the major mechanisms governing the dynamics.

The other important feature of the flow is the so-called Ekman pumping, described in detail in Greenspan (1968). This is an interaction with the Ekman layer through vertical velocities at the top of the boundary layer induced by the inviscid interior flow. Since $R \ll 1$, the Ekman layer is in local equilibrium with the interior flow, and the pumping velocities can be easily calculated. Integration of the Ekman layer equations together with the continuity equation gives the pumping velocity,

$$w_E = \frac{1}{2\Omega\rho} \left(\frac{\partial \tau_y}{\partial x} - \frac{\partial \tau_x}{\partial y} \right) \quad (2.1)$$

where (τ_x, τ_y) is the surface stress, and ρ is the density.

Equation (2.1) is generally valid for either laminar or turbulent Ekman layers, see Charney and Eliassen (1949). The laminar Ekman layer equations are linear, so w_E can be related to the free stream velocity at the top of the boundary layer, (\tilde{u}, \tilde{v}) , giving

$$w_E = -\frac{\rho}{2} \left(\frac{\partial \tilde{v}}{\partial x} - \frac{\partial \tilde{u}}{\partial y} \right) \quad (2.2)$$

A similar relation can be obtained for the turbulent layer provided the free-stream perturbations are much smaller than U_g . Suppose the turbulent shear stress is described by a geostrophic drag coefficient C_g , giving

$$(\tau_x, \tau_y) = C_g \rho U_g^2 (\cos \alpha, \sin \alpha) \quad (2.3)$$

for the undisturbed flow, where α is the angle between the surface stress and U_g the geostrophic wind. Then if the free-stream velocity is perturbed to $(U_g + u, v)$, an expression for w_E accurate to first order in the perturbation velocities is obtained from (2.1) as

$$w_E = \frac{C_g U_g}{2 \Omega} \left(\frac{\partial u}{\partial x} \sin \alpha - \frac{\partial v}{\partial x} \cos \alpha + 2 \frac{\partial u}{\partial y} \cos \alpha \right) \quad (2.4)$$

Since the turbulent boundary layer formulation does not fundamentally change the nature of the Ekman pumping for small perturbations, we will use the laminar relation (2.2) in view of its simplicity.

For the system considered here, with $R \ll 1$ and $E \ll 1$ the interior flow is governed by the vorticity equation

$$\frac{u}{U_g} \frac{\partial}{\partial x} \left(\int + \frac{S}{DR} \right) + \frac{v}{U_g} \frac{\partial}{\partial y} \left(\int + \frac{S}{DR} \right) = \frac{E}{R} \int \quad (2.5)$$

(Ingersoll 1969)

where $\int = \frac{L}{U_g} \left(\frac{\partial v}{\partial x} - \frac{\partial u}{\partial y} \right)$ is the dimensionless interior vorticity, and $S(x,y)$ is the height of the topography. In order to apply equation (2.5) with a flat lower boundary, we require $h \ll D$, where h is the maximum height of the topography.

We can linearise (2.5) by assuming the perturbation velocities are much smaller than U_g . Equation (2.5) shows that the magnitude of the velocity perturbations is of order $\delta = \frac{h}{DR}$ (Hide, 1961) so δ must be small for the linearisation to be valid.

Recalling that for $R \ll 1$, pressure is related to vorticity by the Poisson equation, $\int = \nabla^2 \bar{p}$, it can then be shown that the average pressure force per unit area acting on the sinusoidal corrugation

$$S(x, y) = h \cos(kx + ly)$$

$$\text{is } F = \frac{2 h^2 \Omega^3 \delta}{D^2 U_g K^2 (1 + \Omega^2 \delta^2 / D^2 U_g^2 K^2)} \quad (2.6)$$

in dimensional terms, where $K^2 = k^2 + l^2$

Due to the linearity of the boundary layer equations the surface stress is proportional to the mean velocity in the interior. The continuity equation implies this cannot vary since there is no vertical variation of the velocity field. Thus the average viscous stress is unchanged and the relative change in the total force on the surface compared to the undisturbed value is

$$\frac{F}{F_0} = \frac{2 h^2 \Omega^2}{D^2 u_g^2 k^2} \quad (2.7)$$

where we have assumed E/R is small.

For topography of height 10^3 m, with D taken to be 10 km in the atmosphere, equation (2.7) implies that a length scale of order 6000 km is necessary for the drag to be significantly changed. Topography on this scale is adequately resolved in general circulation models, so this type of interaction should be treated reasonably accurately.

Finally, it may be noted that for the flow over a two-dimensional ridge the restriction $\delta \ll 1$ is not necessary for the validity of the linearisation; we only require $h \ll D$.

(b) Stratified case

We now consider the flow of a stratified, Boussinesq fluid over topography, assuming the Brunt-Vaisala frequency is constant. The flow geometry is the same as in the homogeneous problem, except that a vertical scale is now determined by the stratification. The vertical scale will be $\sim L_f/N$ provided this is much smaller than D . In this case, the algebra is simplified by assuming the fluid occupies the upper half-space, $z > 0$. Note that the homogeneous theory is valid when $L_f/N \gg D$.

The flow will have an inviscid interior, with an Ekman layer on the lower boundary provided the stratified analogue of the Ekman number,

$$E_s = \frac{\delta N}{L_f} \ll 1. \quad \text{We assume } R \ll 1 \quad \text{and the further assumption that}$$

$$E = \frac{h N}{L_f} \ll 1 \quad \text{allows us to consider the lower boundary of the}$$

inviscid flow as horizontal. These three conditions imply that the lower boundary condition for the inviscid flow is obtained by applying the Ekman pumping formula (2.2) at $z=0$.

Assuming the velocity perturbations are small, we can linearise the equations of motion in the interior to give

$$\left. \begin{aligned} U_g \frac{\partial u}{\partial x} - f v &= -\frac{\partial p}{\partial x} \\ U_g \frac{\partial v}{\partial x} + f u &= -\frac{\partial p}{\partial y} \\ U_g \frac{\partial w}{\partial x} &= -\frac{\partial p}{\partial z} - \sigma \\ U_g \frac{\partial \sigma}{\partial x} - N^2 w &= 0 \\ \frac{\partial u}{\partial x} + \frac{\partial v}{\partial y} + \frac{\partial w}{\partial z} &= 0 \end{aligned} \right\} \quad (2.8)$$

where (u, v, w) is the velocity perturbation, p is the perturbation from the hydrostatic pressure, and the buoyancy $\sigma = \frac{g \rho}{\bar{\rho}}$ where $\bar{\rho}$ is the density perturbation from the basic stratification $\rho_0(z)$. Equations (2.8) are those presented by Queney (1947).

The linearised lower boundary condition of Queney is modified to include the effects of Ekman pumping, giving

$$w = U_g \frac{\partial h}{\partial x} - \frac{f}{2} \left(\frac{\partial v}{\partial x} - \frac{\partial u}{\partial y} \right) \quad \text{at } z=0 \quad (2.9)$$

These equations are solved by application of the Fourier transform

$$f^*(k, l, z) = \iint f(x, y, z) e^{-i(kx + ly)} dx dy$$

It follows that

$$u^* = u'(k, l) e^{i m z} \quad \text{etc}$$

and (2.8) gives the inertia-gravity wave dispersion relation

$$m^2 = - \frac{N^2 k^2}{f^2} \frac{(1 - u_g^2 k^2 / N^2)}{(1 - u_g^2 k^2 / f^2)} \quad (2.10)$$

(2.10) can be simplified by the additional assumption $u_g k / N \ll 1$ which, together with the assumption $R \ll 1$ (ie. $u_g k / f \ll 1$), implies

$$m = i \frac{N k}{f} \quad (2.11)$$

where the positive root has been chosen to give exponential decay at infinity.

With a little linear algebra, and the maintenance of our assumptions that $\frac{u_g k}{N}$, $\frac{u_g k}{f} \ll 1$, it can be shown that

$$\begin{aligned} w' &= \frac{i k u_g h'}{(1 + \frac{1}{2} i \frac{f N k}{u_g k})} ; & v' &= \frac{N}{u_g k} w' \\ u' &= - \frac{f N}{k u_g k} w' ; & p' &= - \frac{i N f w'}{k u_g} \end{aligned} \quad (2.12)$$

where $h'(k, \ell)$ is the two-dimensional Fourier transform of $S(x, y)$. Equation (2.12) shows that the magnitude of the velocity perturbations is of order Nh (provided $\delta N/u_g$ is small), therefore we require $\frac{Nh}{u_g} = \frac{\epsilon}{R} \ll 1$ for validity of the linearisation. Note as before that this restriction does not apply to the two-dimensional case, where $\epsilon \ll 1$ is the only requirement.

The form of the solution is fairly straightforward; all the fields are a maximum at $z=0$ with a characteristic decay with height. In the two-dimensional case the vertical velocity at $z=0$ is given by the slope of the hill with a phase shift dependent on the magnitude of the viscous effect. The u perturbations are $O(R)$ and negligible, but the v perturbations remain $O(Nh)$ and are simply related to the shape of the hill. The v field has the characteristic shape it takes in the homogeneous problem discussed before, being positive upstream and negative downstream. When this v field is matched onto an Ekman layer solution which will have positive v , the overall solution will contain a positive jet upstream.

The average pressure drag per unit area for a single Fourier component is easily calculated as

$$F = \frac{|h'|^2 N^2 \oint \delta}{u_g \left(1 + \frac{\delta^2 N^2 k^2}{4 u_g^2 R^2} \right)} \quad (2.13)$$

and the ratio of this stress to the undisturbed stress is

$$\frac{F}{F_0} = \frac{2 N^2 |h'|^2}{u_g^2} \quad (2.14)$$

when $E_s \ll R$

The total change in viscous stress on the surface can be shown to be $O(E_s F)$, and is therefore neglected.

For the two-dimensional case, the total force per unit width can be written as

$$F = \frac{N^2 f \delta}{U_g \left(1 + \frac{\delta^2 N^2}{4 U_g^2}\right)} \int_{-\infty}^{\infty} S^2(x) dx \quad (2.15)$$

With regard to a turbulent boundary layer, it is worth noting that since (2.12) shows $|u'| \ll |v'|$ in the two-dimensional case, the turbulent Ekman pumping term (2.4) is identical to the laminar case with δ replaced by $C_g U_g \cos \alpha / \Omega$. It follows that the term $\frac{1}{4} \left(\frac{\delta N}{U_g}\right)^2$ in the denominator becomes $\frac{1}{4} \left(\frac{C_g N \cos \alpha}{\Omega}\right)^2$ which for almost all atmospheric situations is significantly smaller than unity. Thus for the turbulent boundary layer,

$$F \approx 2 C_g N^2 \cos \alpha \int_{-\infty}^{\infty} S^2(x) dx$$

which is independent of U_g .

In relating this theory to the atmosphere, we should note that when $m^{-1} = f/NK$ is of order 10 km, ie $L \sim 2\pi \times 10^6 m$ effects due to the scale height of the atmosphere and due to the tropopause become significant. For these length scales, the homogeneous theory has some relevance, and numerical models of the atmosphere would be expected to be successful in resolving the main processes.

Equation (2.14), with $h = 10^3 m$, $N = 10^{-2} s^{-1}$ and $U_g = 10 m s^{-1}$ implies a 50% increase in the total stress, on all length scales. When $R \sim 1$ the horizontal scales are of order hundreds of kilometres, and the

vertical scales are roughly 1 km. Such motions are not adequately resolved by general circulation models, and the h^2 dependence of the drag precludes simple representation through smoothing the topography.

In a recent paper Buzzi and Tibaldi (1977) attempted to investigate stratified flows over topography with Rossby number not much less than unity. Part of their theory included viscous effects at small Rossby number, and corresponds to the theory here with the extra restriction $E_s / R \ll 1$. The flow fields they presented are generally misleading. The authors correctly state that their solution is only valid for $R \ll 1$, but fail to recognise that the inertia-gravity wave dispersion relation (our equation (2.10)) implies a wavelike solution when a Rossby number based on wavenumber is > 1 , i.e. Buzzi and Tibaldi's Rossby numbers are misleading by a factor of 2π . The evanescent structures in figures 3 and 4 of their paper consequently omit an important contribution from inertia-gravity waves. Buzzi and Tibaldi also consider a Rossby number expansion of the linearised, inviscid problem, with the stated objective of identifying ageostrophic effects for finite Rossby number. This approach is quite unnecessary as their, and indeed the non-hydrostatic, equations derived by Queney (equations (2.8) above) can be readily solved for any value of Rossby number by Fourier transform methods.

3. The numerical model.

The work described here is not intended to model atmospheric flow but has been deliberately idealised so as to illustrate the role of basic processes. It has been developed for studying scales smaller than those considered here and is probably more general than necessary for the present study. The numerical method of representing topography and details of the numerical model are described in Mason and Sykes (1977) and will not be presented here.

The model equations are those for a two-dimensional incompressible Boussinesq fluid.

$$\frac{\partial u}{\partial t} + u \frac{\partial u}{\partial x} + w \frac{\partial u}{\partial z} = -\frac{\partial p}{\partial x} + f v + \frac{\partial}{\partial x} (2 \nu_H \frac{\partial u}{\partial x}) + \frac{\partial}{\partial z} (\nu_0 \frac{\partial u}{\partial z} + \nu_H \frac{\partial w}{\partial x}) - (u - u_g) / T(z) \quad (3.1)$$

$$\frac{\partial v}{\partial t} + u \frac{\partial v}{\partial x} + w \frac{\partial v}{\partial z} = -\frac{d p_0}{d y} - f u + \frac{\partial}{\partial x} (\nu_H \frac{\partial v}{\partial x}) + \frac{\partial}{\partial z} (\nu_0 \frac{\partial v}{\partial z}) - v / T(z) \quad (3.2)$$

$$\frac{\partial w}{\partial t} + u \frac{\partial w}{\partial x} + w \frac{\partial w}{\partial z} = -\frac{\partial p}{\partial z} - \frac{g \beta}{f} + \frac{\partial}{\partial x} (\nu_H \frac{\partial w}{\partial x} + \nu_0 \frac{\partial u}{\partial z}) + \frac{\partial}{\partial z} (2 \nu_0 \frac{\partial w}{\partial z}) - w / T(z) \quad (3.3)$$

$$\frac{\partial \theta}{\partial t} + u \frac{\partial \theta}{\partial x} + w \frac{\partial \theta}{\partial z} = \frac{\partial}{\partial x} (K_H \frac{\partial \theta}{\partial x}) + \frac{\partial}{\partial z} (K_0 \frac{\partial \theta}{\partial z}) - (\theta - \theta_0(z)) / T(z) \quad (3.4)$$

$$\frac{\partial u}{\partial x} + \frac{\partial w}{\partial z} = 0 \quad (3.5)$$

with boundary conditions $u = v = w = 0$ on the lower boundary $z = S(x)$ and

$\frac{\partial u}{\partial z} = \frac{\partial v}{\partial z} = w = 0$ on the upper boundary $z = D$ (see figure 1).

$\frac{dP_0}{dy}$ is the background pressure gradient responsible for the geostrophic flow.

The domain is periodic in the x direction and the boundary conditions on the

density are $\rho = \frac{\bar{\rho}}{g} N^2 S(x)$ on $z = S(x)$ and $\rho = \frac{\bar{\rho}}{g} N^2 D$ at $z = D$.

The basic density profile is $\rho_0(z) = \frac{\bar{\rho}}{g} N^2 z$ and $T(z)$ denotes the

Rayleigh damping coefficients mentioned below. ν_0 and k_0 are the coefficients of vertical diffusion and ν_H and k_H those of horizontal diffusion.

The form of the viscous terms is obtained from consideration of the stress tensor, which is $\nu \left(\frac{\partial u_i}{\partial x_j} + \frac{\partial u_j}{\partial x_i} \right)$ in an isotropic fluid. Since we are specifically interested in surface stresses, any anisotropy introduced for sub-grid parameterisation must be used to define the stresses rather than the stress gradients. If a horizontal diffusion coefficient is associated with horizontal derivatives in the definition of the stress tensor, then the momentum equations (3.1)-(3.3) follow immediately.

We intended to impose a form of radiation boundary condition at $z = D$ but methods described in the literature (eg Orlanski 1976) do not seem able to cope with gravity waves (whose group velocity is oppositely directed to their phase velocity) leaving the domain at arbitrary angles. We experimented with these and other methods and finally found the use of Rayleigh damping on the uppermost 6 levels to be most satisfactory. The coefficient $T^{-1}(z)$ doubles between grid levels reaching a maximum value at $z = D$. With a sensible choice of the maximum value this method is highly effective in simulating a radiation condition for waves, but cannot be used where evanescent disturbances reach the damping levels. In such cases the Rayleigh damping gives rise to an unphysical pressure force on the hill. For the scales of motion considered here it follows that Rayleigh friction can be applied when the fluid is sufficiently stratified but under near neutral conditions a stress free rigid upper boundary is preferable.

The numerical model used here contains no implicit smoothing (either temporal or spatial) and consequently it is natural to expect the topographic forcing to give some energy in grid length waves. With an isotropic fluid viscosity these waves have a typical amplitude of less than a few percent of that of the main features. In the results presented here an anisotropic

fluid viscosity has been posed so that ν_0 is associated with vertical diffusion and ν_H with horizontal diffusion (likewise K_0 and K_H for thermal diffusivity). The values assigned to ν_H (and K_H) give a grid Reynolds number $U_g \Delta x / \nu_H = 20$ where Δx is a horizontal grid spacing. This reduces the grid length waves to an imperceptible value but gives completely negligible dissipation of other motions which occur on the scale presented here. The use of anisotropic fluid viscosities can, if desired, be justified on the basis of ideas concerning energy cascades and on atmospheric observations (Lumley and Panofsky 1964) of the horizontal velocity variance and the spectral scale of the horizontal motions. In consequence of better resolution the examples given in Mason and Sykes (1977) demonstrated an absence of grid length waves with $\nu_H = \nu_0$.

The starting procedure for the model consisted of setting the flow everywhere above $S(x)$ to be independent of x and equal to the one-dimensional Ekman boundary layer solution. Though abrupt this procedure did not give rise to any unreasonable motion or lead to numerical difficulties. Allowing the hill to appear gradually seemed to have no advantages and wasted computation time.

4. Results

In this section we describe some results obtained with the numerical model of § 3. The hill considered has shape $S(x) = h \cos^2(\pi x/b)$ for $|x| < b/2$ and $S(x) = 0$ otherwise. In all the cases presented $b = 0.25L$ where L is the horizontal length of the domain, and $h = 10^3$ m. The depth of the domain D has been taken to be 10 km in the runs with uniform density and 15 km in the runs with a basic stable density gradient. In the latter cases the Brunt-Vaisala frequency is constant and equal to 10^{-2} s^{-1} . The Coriolis parameter f has been taken to be 10^{-4} s^{-1} and the vertical coefficients of diffusion ν_v and K_0 are both $5 \text{ m}^2 \text{ s}^{-1}$ implying an Ekman layer depth, $\delta = 330$ m. The background pressure gradient is chosen to give $U_g = 10 \text{ m s}^{-1}$.

The important dimensionless parameters we shall use are a Rossby number $R = 2\pi U_g/bf$, a Froude number Nh/U_g and an Ekman number $E_s = \delta N/fb$ when the fluid is stratified or $E = \delta/D$ otherwise. For the flows presented below $Nh/U_g = 0$ or 1 and R and E_s are proportional to L^{-1} .

a. Homogeneous Flows

We have computed the homogeneous flows for cases with $R = 10, 3, 1$ and 0.3 . These flows are not very interesting and here we only illustrate the flow for $R = 1$. Figures 2a and b show the streamlines and the transverse component of velocity V , 7 days after the start of the integration. The system has a number of characteristic time scales, viz f^{-1} , L/U_g and $2(Ef)^{-1}$, and a steady state requires integration over periods longer than the spin-up time $2(Ef)^{-1}$ which in this case is about 7 days. The fields presented are not completely steady but the small remaining time dependence does not materially effect any of the results presented.

The features of figures 2a and b are characteristic of flow at small Rossby number. The interior flow is independent of height and the transverse velocity component shows the features of the vortex stretching mechanism discussed in § 2. The details of the flow show some effects due

to inertial forces. It follows from the low Rossby number solution that the pressure is a maximum above the summit of the hill and fluid is thus accelerated in the positive x-direction in the lee of the hill. This is contrary to the aerodynamic situation where the pressure minimises over the hill, and here the surface stress maximises on the lee slope of the hill and again downstream. The variations in surface stress are about $\pm 20\%$ of the undisturbed value.

b. Stratified Flows

Figures 3-6 illustrate flows for Rossby numbers $R = 0.3, 1, 3$ and 10 respectively. Figure 3a shows the streamlines over a hill of length $2 \cdot 10^6$ m ($R = 0.3$) and Figure 3b shows the corresponding transverse component of velocity. As in the homogeneous case a steady state requires integration for the spin up time ($2 (E_s f)^{-1}$) which for the longest scale disturbances is about 7 days.

The presence of stratification limits the time step to ~ 30 s (c.f. ~ 200 s used in the homogeneous flows). For $R = 10$ this is consistent with the vertical propagation speed of inertia-gravity waves but for $R = \frac{1}{3}$ it appears to be due to a numerical instability associated with the use of a Du Fort-Frankel treatment of the viscous terms. In the homogeneous case it was possible to demonstrate that use of the Du Fort-Frankel scheme caused the viscous and Coriolis terms to interact giving a slow instability (Mason and Sykes 1977). In the stratified case the empirical evidence suggests a similar slow instability can occur with the buoyancy terms and it may have been erroneously interpreted by other workers (Chan 1976) as a failure of the numerical scheme to conserve energy.

The diagrams illustrate the fields after 2 days and contain a small inertial oscillation. This takes the form of a slight oscillatory movement of the pressure field in the x-direction with frequency f , and although significant errors are introduced into the estimation of steady pressure forces the fields presented here are not sensitive to this feature.

The streamlines for the $R = \frac{1}{3}$ ($b = 2 \times 10^6$ m) case (Fig 3a) appear broadly

similar to the homogeneous flow discussed above but show one major change. The surface stress on the lee slope of the hill is very much increased to nearly twice the undisturbed value. This increased stress is manifest in the streamlines by the proximity of the lowest contour to the surface $S(x)$. The basic stratification inhibits vertical motions forcing the fluid to rise gently upstream and flow over the summit in a vertically constricted jet. On the lee slope the buoyancy forces accelerate the fluid as it returns to its equilibrium level. As we shall see these effects are more pronounced in flow in shorter length scales.

The transverse velocity field shows more changes from the homogeneous case. The scale height of the disturbance is reduced from D to about 3 km and, as discussed in § 2, the magnitude of the transverse velocity is increased. It exceeds the undisturbed boundary layer velocities and completely overwhelms them. The horizontal scale of the disturbance is reduced from that in the homogeneous case as a result of the reduced spin up time $((E_f)^{-1}$ cf $(E_f)^{-1}$). The weak positive maximum downstream of the hill is a transient effect in which the fluid vortex filaments initially on top of the hill have been advected off and stretched. In the steady solution this feature should disappear.

Figures 4a and b illustrate the flow with $R = 1$ ($b = 6 \times 10^5$ m). The streamlines now contain waves which propagate vertically away from the hill and are absorbed by the Rayleigh friction which occurs from $z = 10$ km upwards. The behaviour of the surface stress is much as in the $R = 0.3$ case. In the transverse velocity field a further reduction in height scale to ~ 1 km is visible. As expected from the theory, the magnitude of this velocity component is $\sim Nh$ again, and we conclude that even though the Rossby number is unity the small Rossby number solution describes the essential features.

Figures 5a and b illustrate the flow with $R = 3$ ($b = 2 \cdot 10^5$ m). The streamlines now show more energy in waves and a more dramatic change in surface stress. It falls to near zero at the leading and trailing edges of the hill but near the top of the hill on the lee slope the surface stress reaches a maximum value of almost 5 times the undisturbed value.

The transverse velocity retains some vortex stretching effects in the interior, although waves are clearly present as well. However the maxima in the boundary layer are not expected from inviscid theory; Queney's theory predicts velocities $\sim Nh/R$, which is 3 m s^{-1} here. In the viscous flow there is a significant reduction in the u-component of velocity in the vicinity of the stress minima. Thus in the transverse momentum equation it follows that the basic pressure gradient $\frac{d P_0}{dy}$ is no longer balanced by $f u$ and a consequent acceleration of v is expected.

Figures 6a and b illustrate the flow with $R = 10$ ($b = 6 \times 10^4 \text{ m}$). The additional feature of the streamlines here is the strong, almost symmetric, separation bubbles either side of the hill. The maximum surface stress is about 5 times the undisturbed value. The transverse velocity field shows no evidence of vortex stretching but contains maxima of nearly 10 m s^{-1} . The mechanism for this maxima is as discussed for figure 5b but now flow separation is important in imposing a sufficiently long length scale for the transverse acceleration to occur.

Flow trajectories

In the homogeneous flows considered here the flow directions in the interior and boundary layer are not much changed by the presence of topography. The corresponding stratified flows show marked changes; a characteristic feature is a low-level transverse jet on the upwind slope of the topography. Figure 7 illustrates particle trajectories at $R = 1$. The trajectories originate at 300 m and 900 m above the surface upstream of the hill. The homogeneous flow trajectory at 300 m is nearly unaffected by the topography and maintains an almost constant angle to the geostrophic wind. At 900 m the small topographically induced transverse component is evident. However the stratified flow at 300 m shows a marked deviation in mean direction, giving a net displacement of 320 km. At 900 m the final displacement is small but the local effects could be significant.

Pressure forces

For the stratified flows, Table I gives values of the total pressure force P and ratio of this pressure force to the undisturbed viscous force F_0 acting on the

width of the hill. In all the cases considered, the total viscous stress on the surface was not significantly changed by the topography. At large Rossby numbers gravity wave drag dominates. From Queney's theory it follows that the pressure force $P = 1.08 U_g N h^2$ for the periodic hills considered here. This is independent of horizontal length (we assumed $2\pi U_g / N L \ll 1$) and is equal to $1.08 \cdot 10^5 \text{ N m}^{-1}$ in good agreement ^{with} the computed forces at $R = 10$. For small Rossby numbers, § 2 predicted the ratio $P/F_0 = 0.626 N^2 h^2 / U_g^2$ for our periodic hills. Table I confirms a tendency to this result at $R = \frac{1}{3}$ and indicates that at $R = 1$, as expected from the inspection of velocity fields, a similar magnitude of force ratio is obtained.

Table II shows the force ratios P/F_0 for the homogeneous flows. Except for $R = \frac{1}{3}$, these are much smaller than the corresponding stratified cases. At $R > 1$ aerodynamic drag is responsible for the pressure force, while for small R § 2 predicted $P/F_0 = 0.0036 \frac{h^2 f^2 L^2}{D^2 U_g^2}$ for our periodic hills. At $R = 1$ this prediction is small but at $R = \frac{1}{3}$ it has a value of 0.26. The computed value at $R = \frac{1}{3}$ is larger, and the difference appears to be due to the finite Rossby number and height of the topography.

Transient forces occur in the computation as the fluid initially on top of the hill is advected off and transported around the periodic domain. The magnitude of the transient is similar to the pressure force in the isolated ridge problem, whose singularity was discussed in § 2, ie. $P = \frac{f^2 h^2 b^2}{8 D}$ for the hills used here. In the stratified flows, the magnitude of this force and the observed transients were small compared with the steady forces.

In the homogeneous flows, the relative magnitude of this transient maximised at $R = 1$, where it was an order of magnitude larger than the steady force. For these cases the estimation of the mean pressure forces necessitated averaging, and at $R = 1$, significantly larger errors were introduced ($\sim 50\%$).

5. Conclusions

We have illustrated flow over topography 1 km high for various length scales in the region of hundreds of kilometres. The results could have been presented in purely dimensionless terms, and identical flow patterns are appropriate to cases

in which all geometric length scales and U_g are reduced by a factor and the viscosity reduced by the square of that factor (ie consistent with a constant geostrophic drag coefficient).

The results show the importance of stratification in determining the flow on these scales. A characteristic feature of the flow was a low-level transverse jet on the upwind side of the hill which would have important consequences for local forecasting and pollution dispersal.

The results concerning forces on this length scale served to emphasise the importance of gravity wave drag when the length scale is not so long as to make the Rossby number unity. When the Rossby number is unity or less the boundary layer dissipation mechanism described in § 2 becomes important and the theory of § 2 provides a good estimate of its magnitude. The one kilometre high topography considered is rather exceptional on length scales for which gravity wave drag is important but on the length scale for which the boundary layer dissipation mechanism is effective ($R \lesssim 1$) this height is by no means uncommon, and leads to an effective doubling of the local momentum transfer.

In forecasting and general circulation models these lengths are generally sub-grid scale, and the parameterisation of the boundary layer dissipation mechanism can in principle be achieved through a surface drag coefficient.

REFERENCES

- Batchelor, G. K. 1967 "An Introduction to Fluid Dynamics", Cambridge University Press.
- Bretherton, F. P. 1969 "Momentum transport by gravity waves", Q. J. Roy. Met. Soc., 95 pp 213-243.
- Buzzi, A. and Tibaldi, S. 1977 "Inertial and Frictional effects on rotating and stratified flow over topography," Q. J. Roy. Met. Soc. 103, pp 135-150.
- Chan, R. K.-C. 1976 "A second order, time integration scheme for calculating stratified compressible flow" J. Comp. Phys., 22, pp 74-86.
- Charney, J. G., and Eliassen, A. 1949 "A numerical method for predicting perturbations of the middle latitude westerlies" Tellus, 1, pp 38-54.
- Eady, E. T. 1949 "Long waves and cyclone waves" Tellus, 13, pp 33-52.
- Greenspan, H. P. 1968 "The theory of rotating fluids", Cambridge University Press.
- Hide, R. 1961 "Origin of Jupiter's Great Red Spot". Nature, 190, pp 213-218.
- Huppert, H. E. & Stern, M. E. 1974 "The effect of side walls on homogeneous rotating flow over 2 dimensional obstacles" J. Fluid Mech., 62, pp 417-436.
- Ingersoll, A. P. 1969 "Inertial Taylor columns and Jupiter's Red Spot", J. Atmos Sci., 26, pp 744-752.
- Janowitz, G. S. 1975 "The effect of bottom topography on a stratified flow in the Beta plane", J. Geophys. Res., 80, pp 4163-4168.

Lumley, J. L. and Panofsky, H. A. 1964 "The structure of atmospheric turbulence"
Interscience Publishers.

Mason, P. J. 1977 "Forces on spheres moving horizontally
in a rotating stratified fluid" Geophys.
Astrophys. Fluid Dynamics, 8, pp 137-154.

Mason, P. J. and Sykes, R. I. 1977 "A simple cartesian model of boundary
layer flow over topography" to appear in
J. Comp. Phys.

Merkine, L. O. 1975 "Steady finite amplitude flow over long
topography in a rotating stratified atmosphere"
J. Atmos. Sci. 32 pp 1881-1891.

Orlanski, I. 1976 "A simple boundary condition for
unbounded hyperbolic flows", J. Comp. Phys.,
21, pp 251-269.

Queney, P. 1947 "The problem of air flow over mountains:
a summary of theoretical studies", Bull. Am.
Meteor. Soc., 29, pp 16-27.

Rhines, P. 1970 "Edge, bottom and Rossby waves in a
rotating stratified fluid",
Geophysical Fluid Dynamics, 1, pp 273-302.

Smith, F. B. 1975 "Turbulence in the atmospheric boundary
layer" Sci. Prog., Oxf. 62, pp 127-151.

Table I Computed net pressure forces for stratified flows

R	10	3	1	$\frac{1}{3}$
$P/N \text{ m}^{-1}$	1.0×10^5	1.2×10^5	0.8×10^5	2.7×10^5
P/F_0	10	4	0.8	0.8

Table II Computed net pressure forces for homogeneous flows

R	10	3	1	$\frac{1}{3}$
P/F_0	0.14	0.03	0.04	0.5

Legends

Figure 1.

Schematic diagram of flow geometry.

Figure 2.

Numerical results obtained with a mesh of 64 by 32 points for homogenous flow with $R = 1$. The results are presented with a uniform spacing between grid points, the actual grid point heights in metres are indicated on the right hand side of the diagram.

(a) shows streamlines, chosen to give an almost uniform spacing in the absence of topography.

(b) shows the transverse component of velocity, contour values are in ms^{-1} .

In this and figures 3-5 we should emphasise that the contour plotting program is based on linear interpolation between grid point values. With the method of representing topography used here (Mason and Sykes 1977) this procedure can produce spurious contours and "wiggles" near the surface.

Figure 3.

Numerical results obtained with a mesh of 64×36 points for a stratified flow with $R = \frac{1}{3}$. See figure 2 for further details.

Figure 4.

As figure 3 but $R = 1$

Figure 5

As figure 3 but $R = 3$

Figure 6

As figure 3 but $R = 10$

Figure 7

Horizontal projection of flow trajectories originating $1.2 \times 10^6 \text{ m}$ upstream of the crest of the hill. The integration domain corresponds to the $R = 1$ examples above ie $L = 2.4 \times 10^6 \text{ m}$ Solid lines

denote trajectories starting at $z = 300_m$ and dashed lines those starting at $z = 900_m$. The heavy lines denote the stratified case and the thin lines the neutral case. The positions of the edges of the hill are indicated by vertical dashed lines.

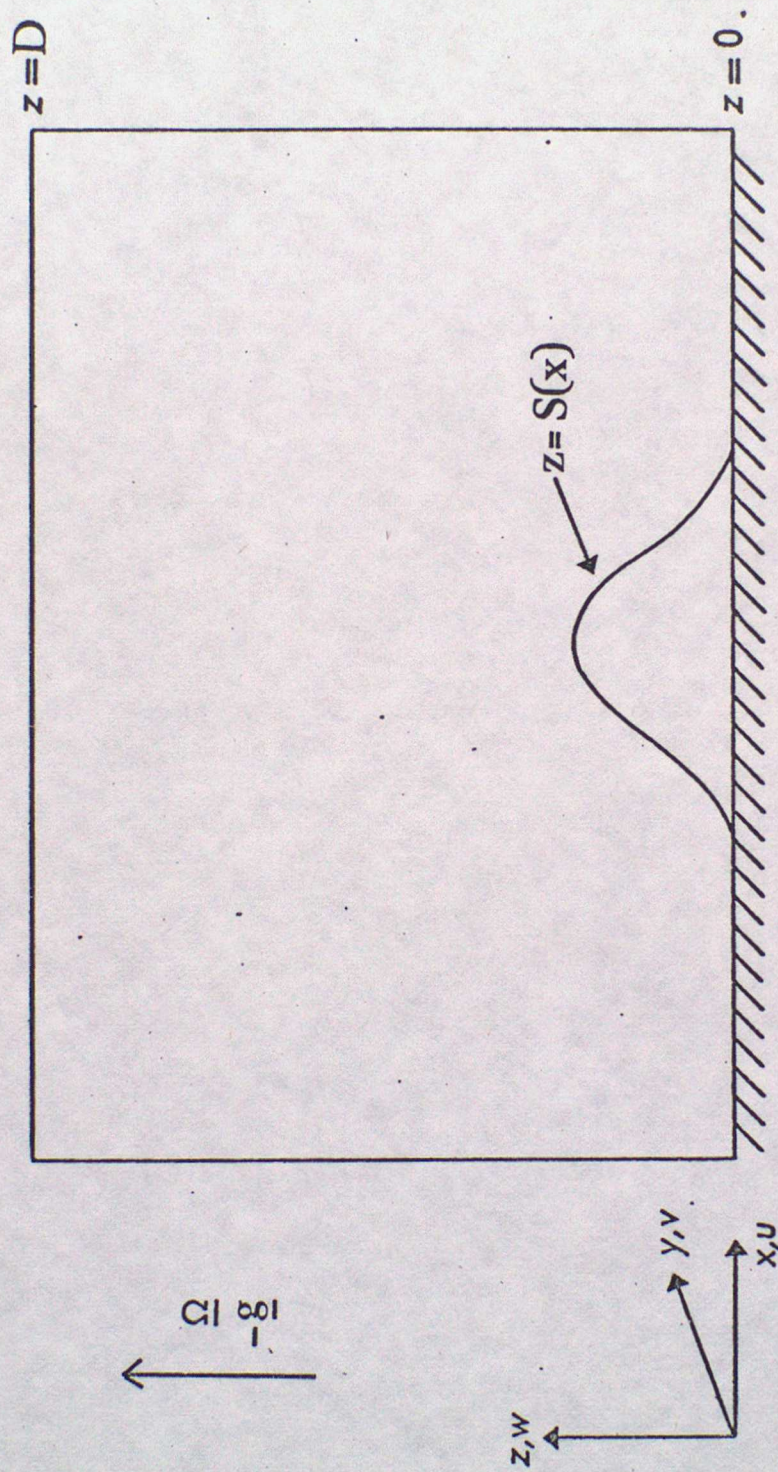
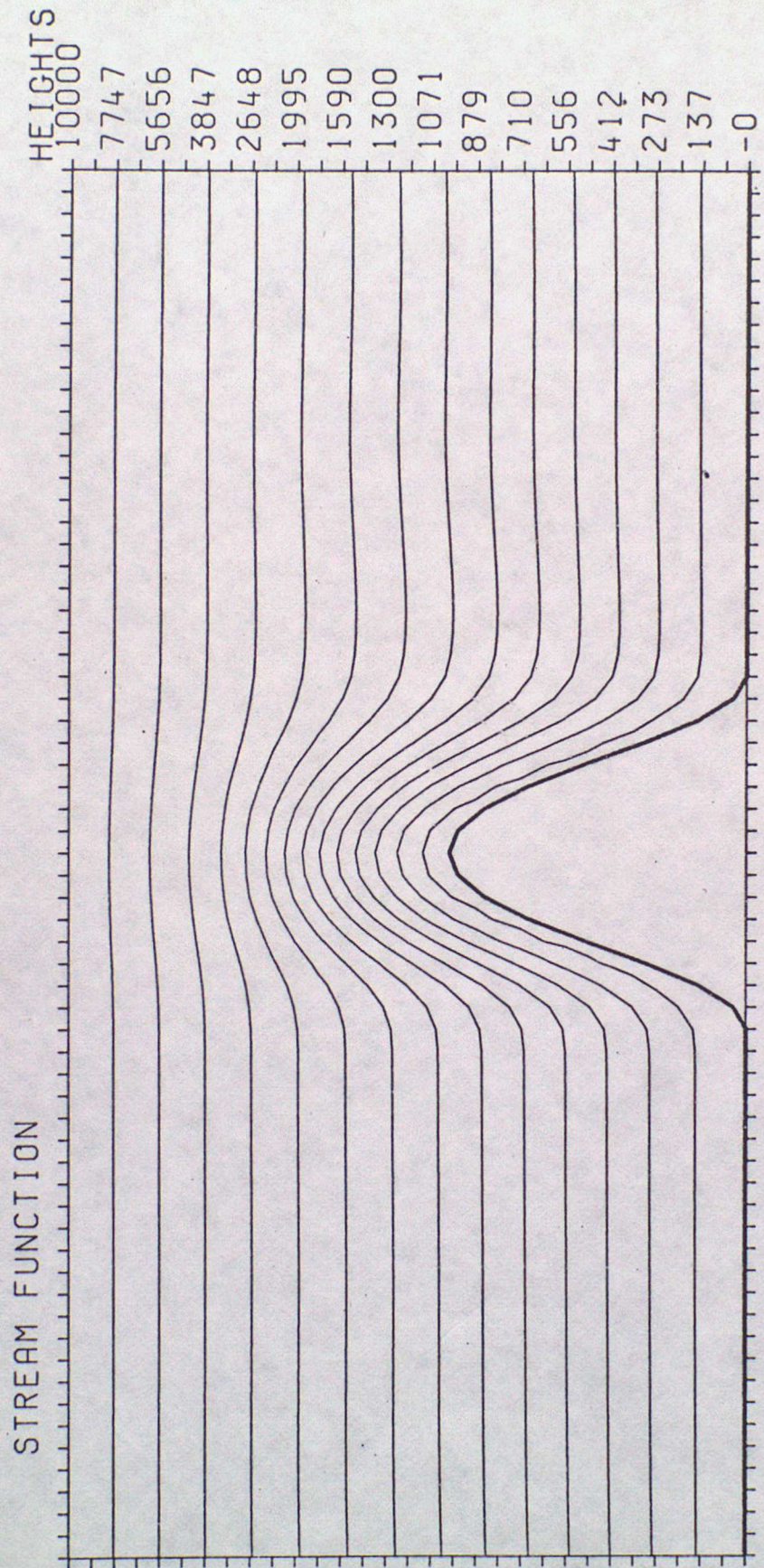


Figure 1

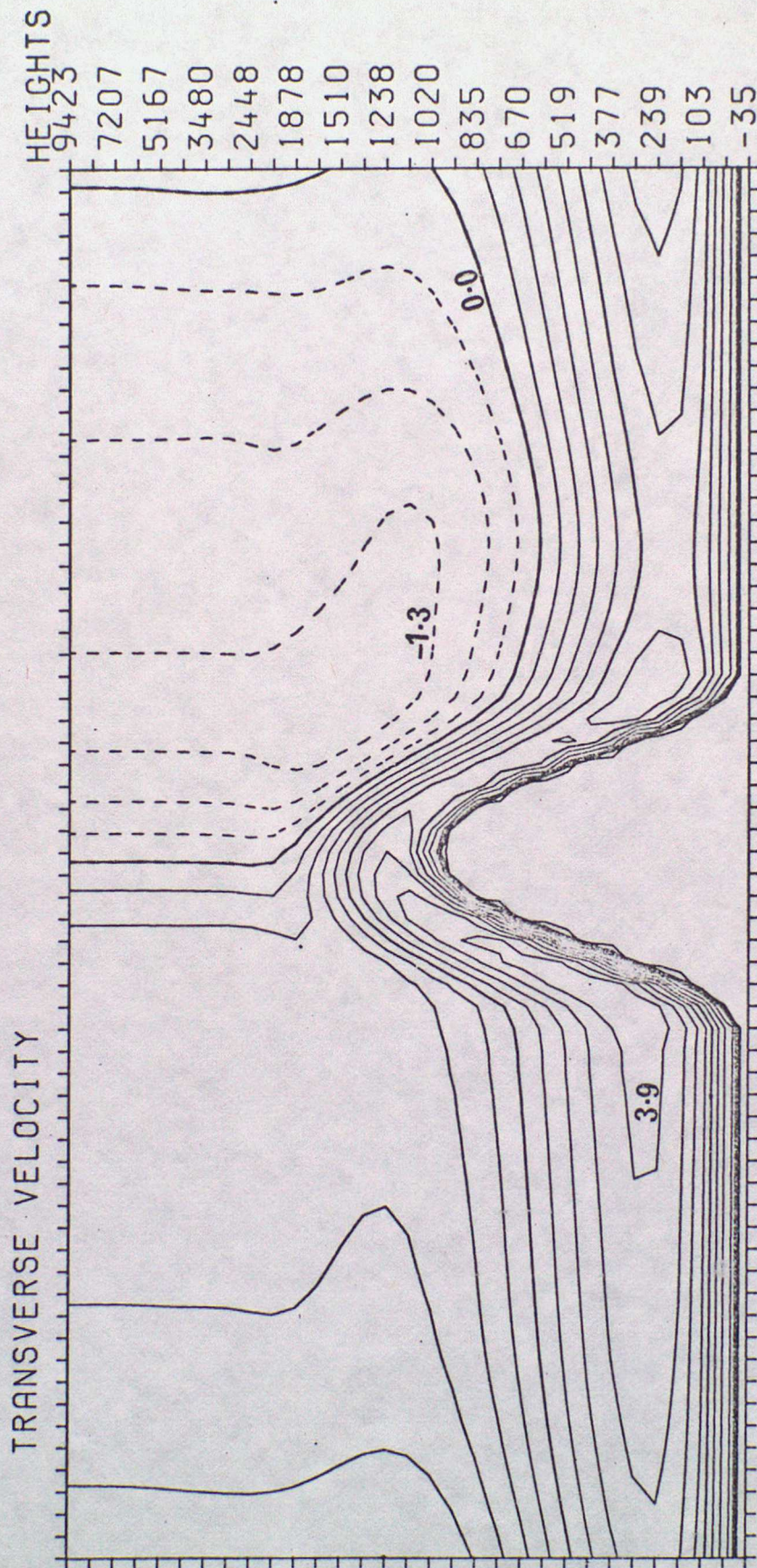
BOX LENGTH=2.400x10⁶



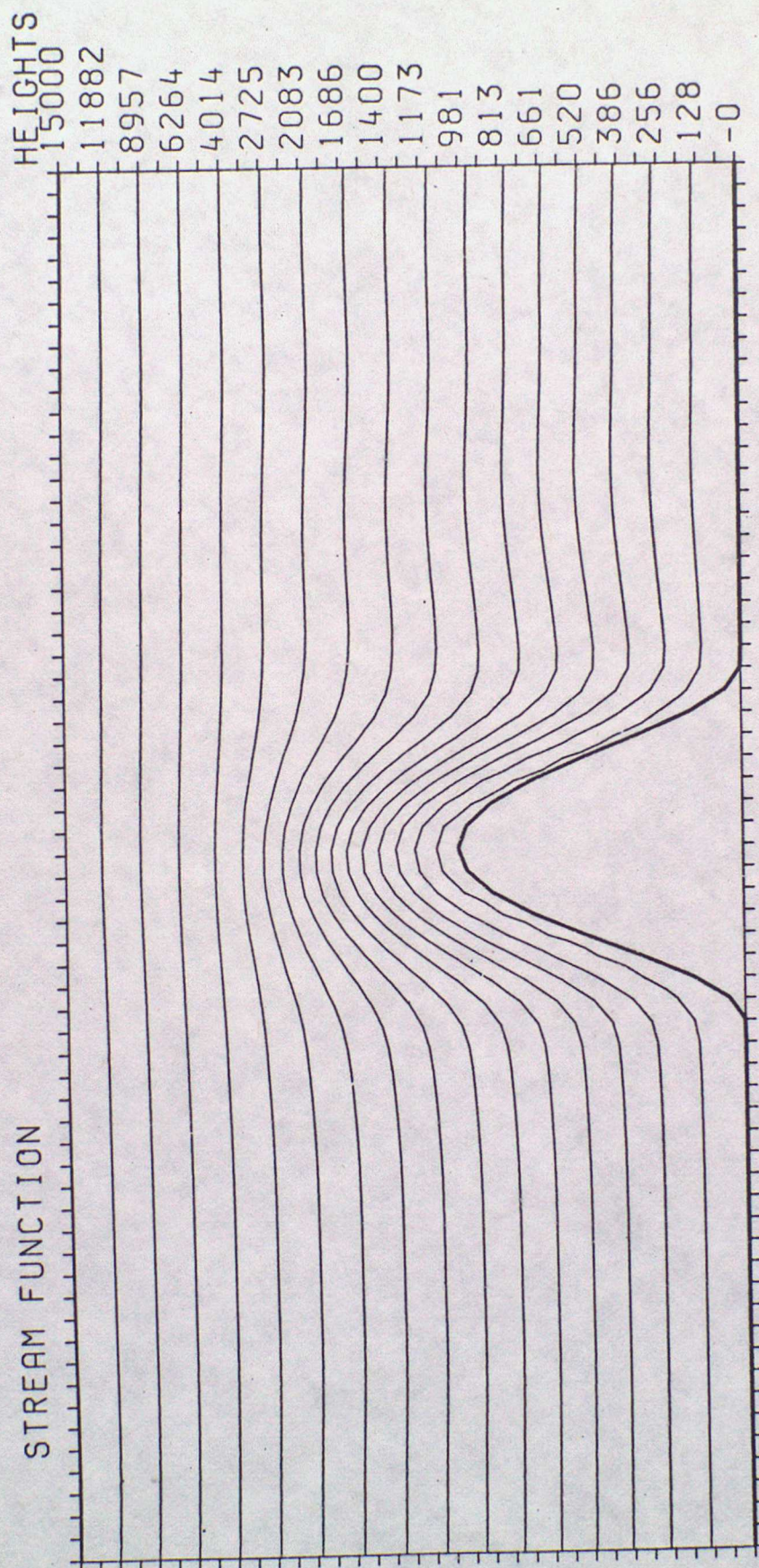
no
units

Fig 2a

BOX LENGTH=2.400x10⁶



BOX LENGTH=8.000x10⁶



BOX LENGTH=8.000x10⁶

TRANSVERSE VELOCITY

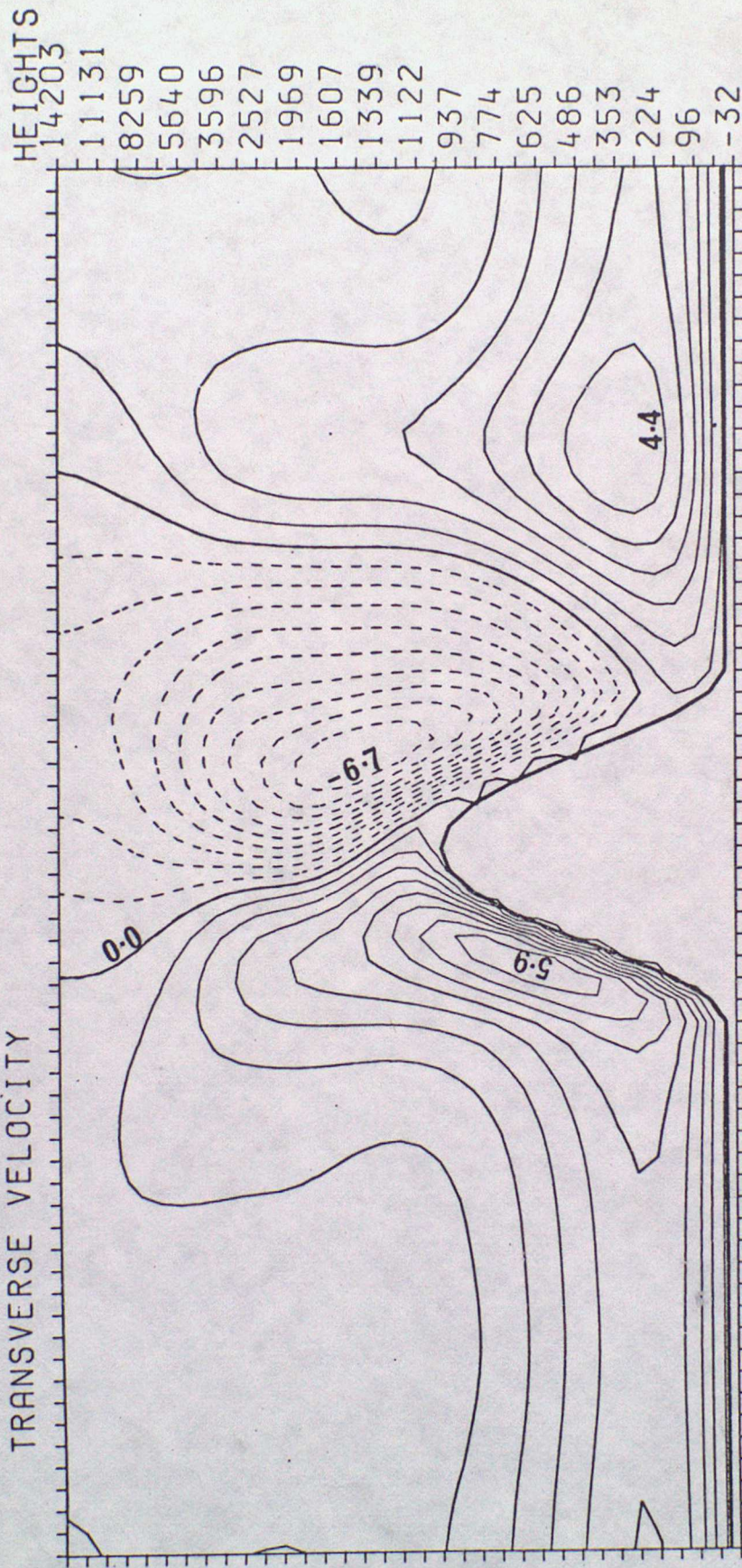


fig 3 b

BOX LENGTH=2.400x10⁶

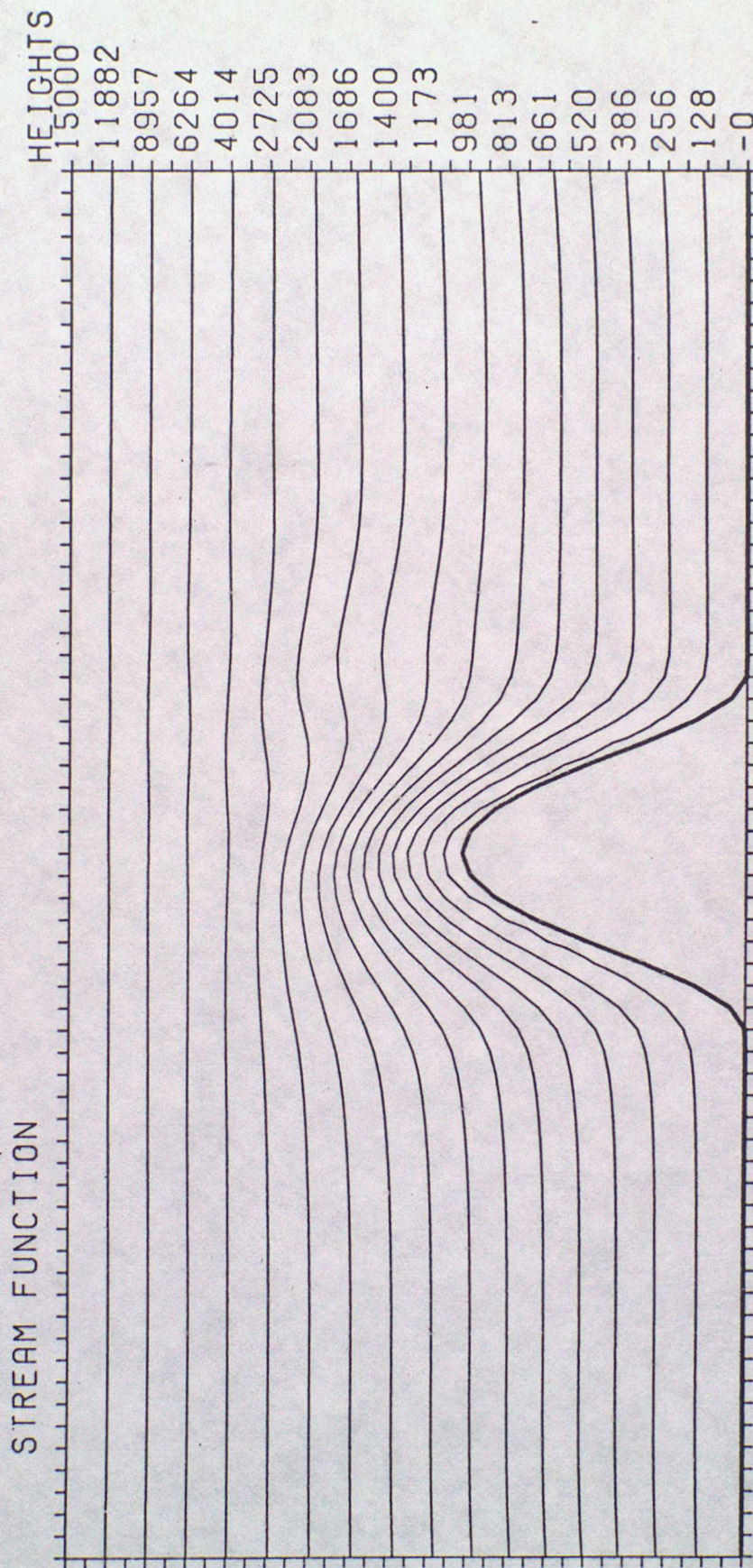


Fig 4a

BOX LENGTH=2.400x10⁶

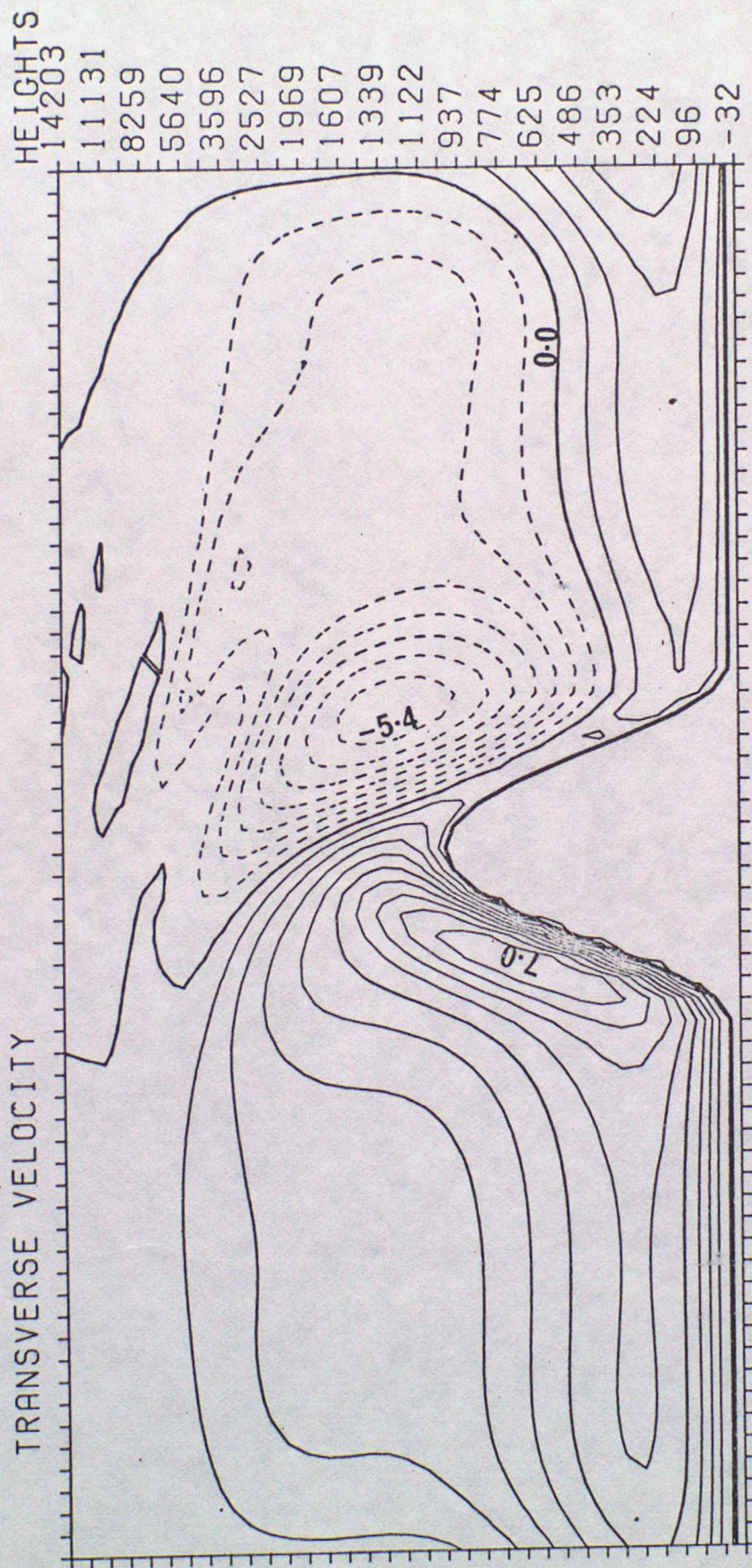


Fig 4b

BOX LENGTH=8.000x10⁵

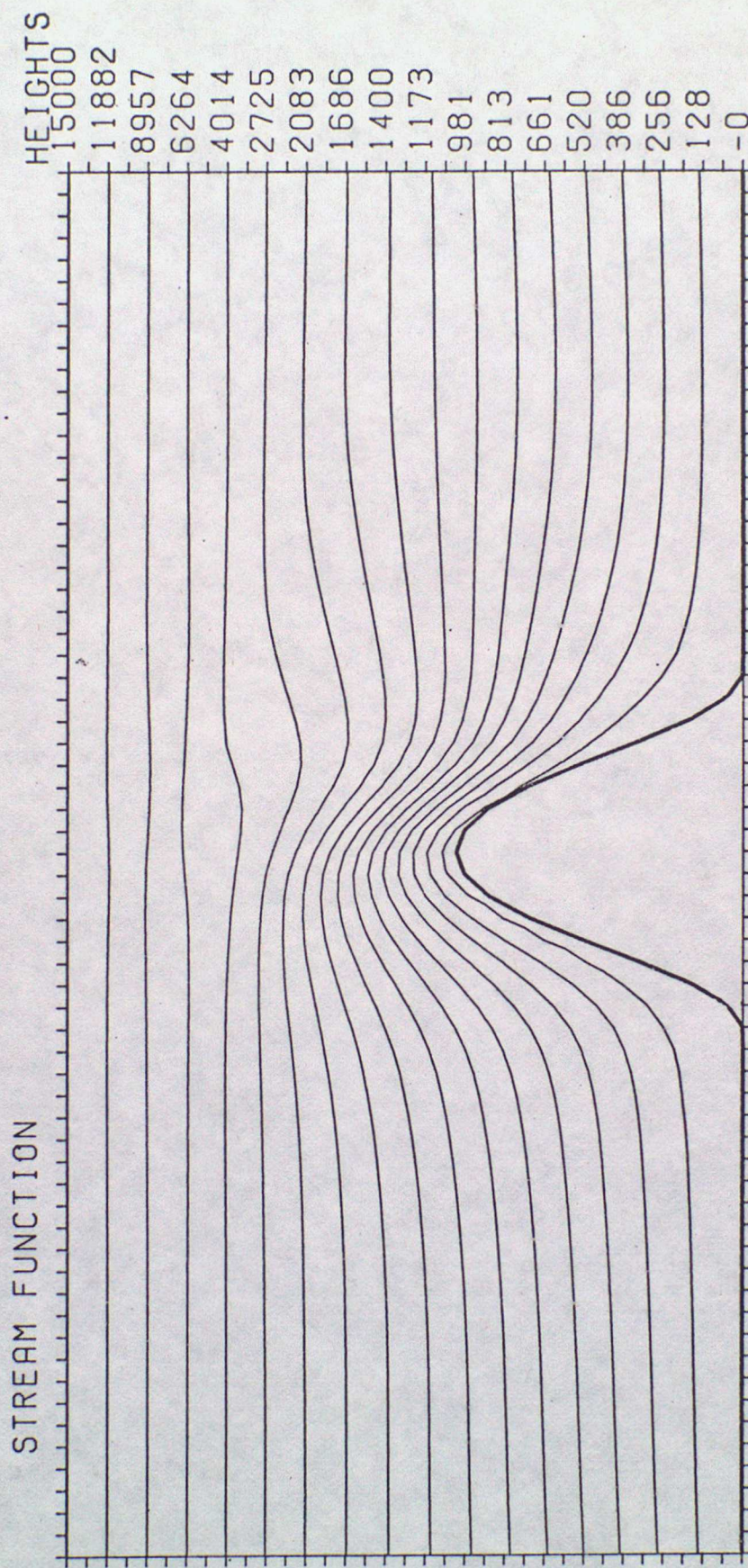


Fig 5a

BOX LENGTH=8.000x10⁵

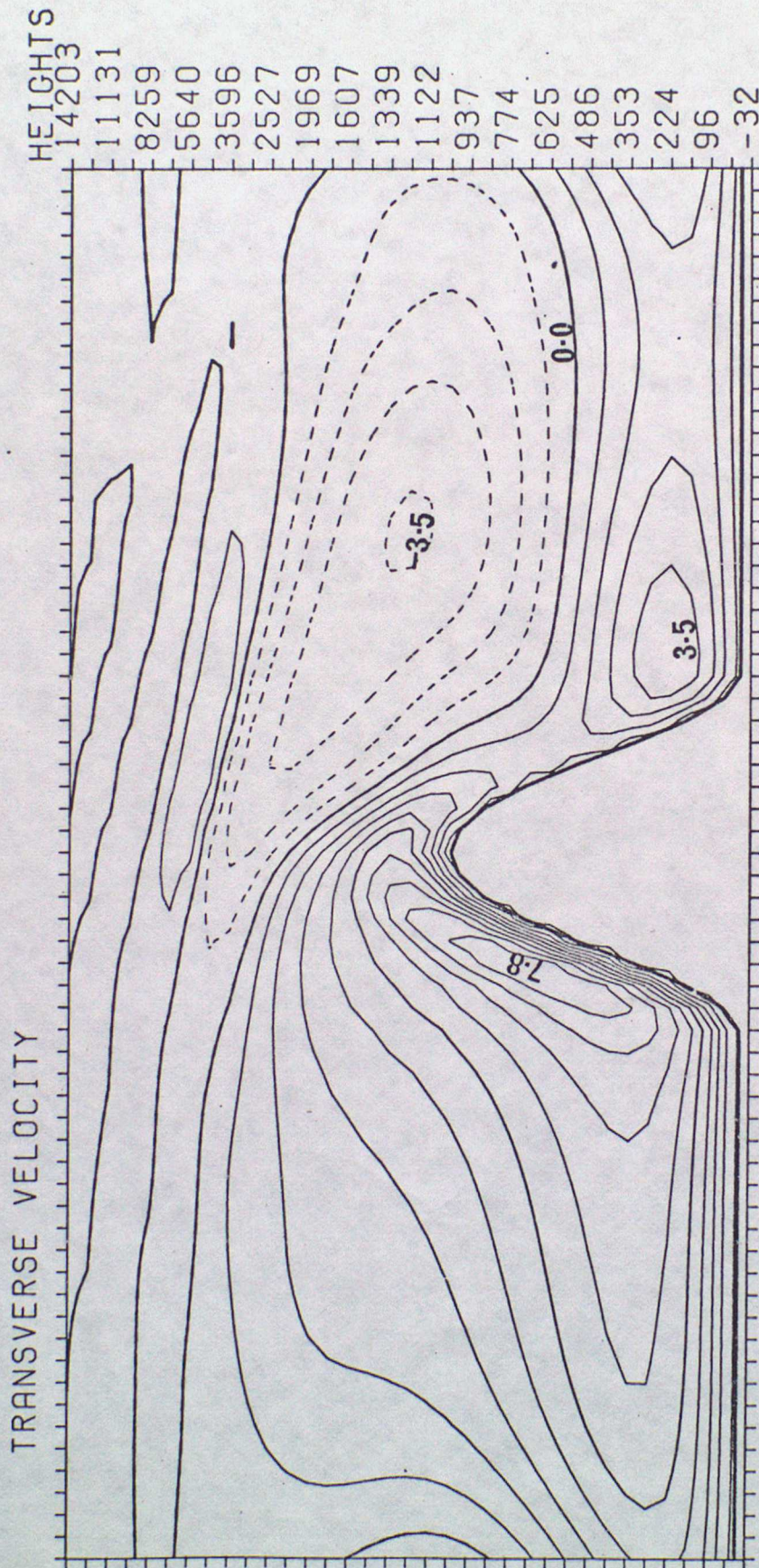


Fig 56

BOX LENGTH=2.400x10⁵

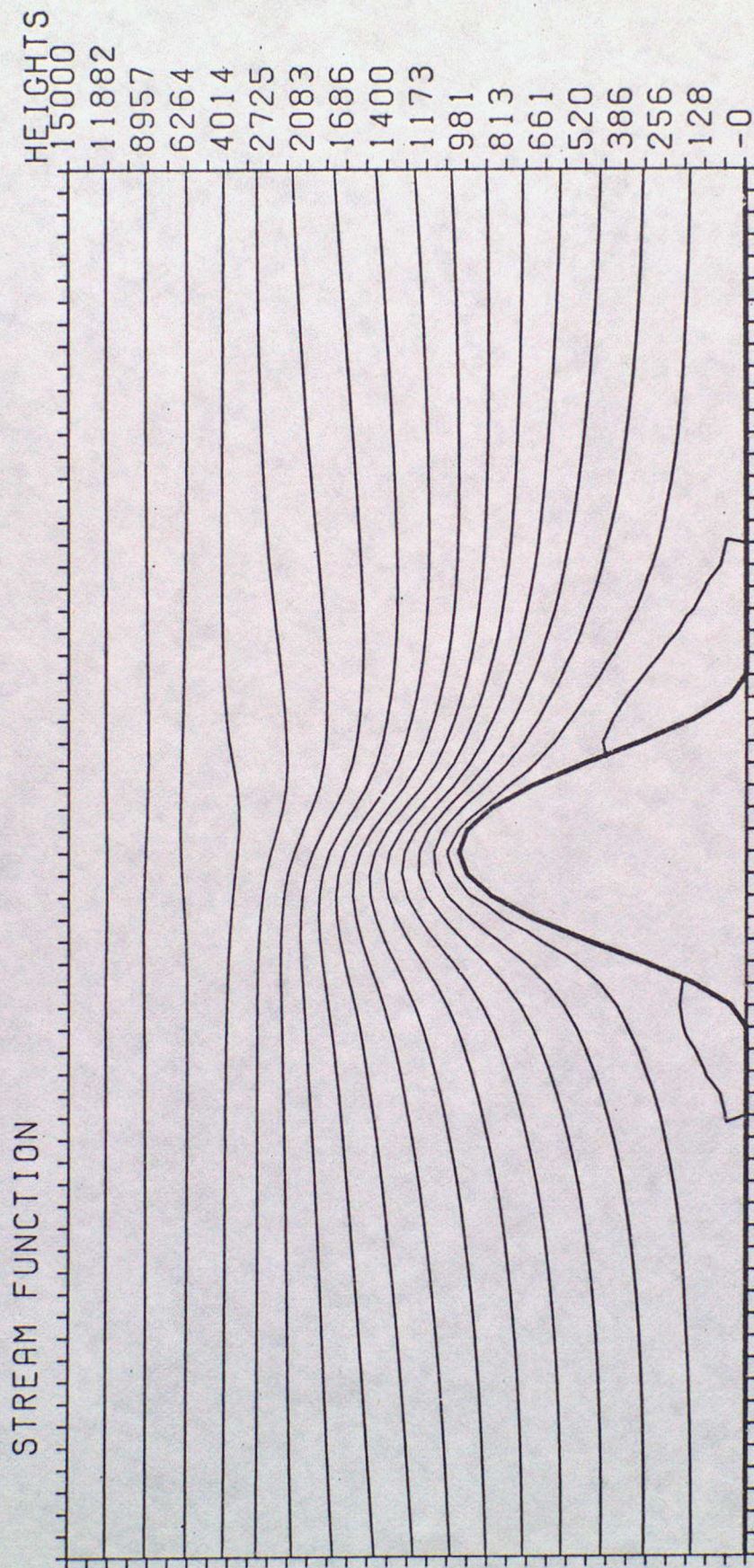


Fig 6a

BOX LENGTH=2.400x10⁵

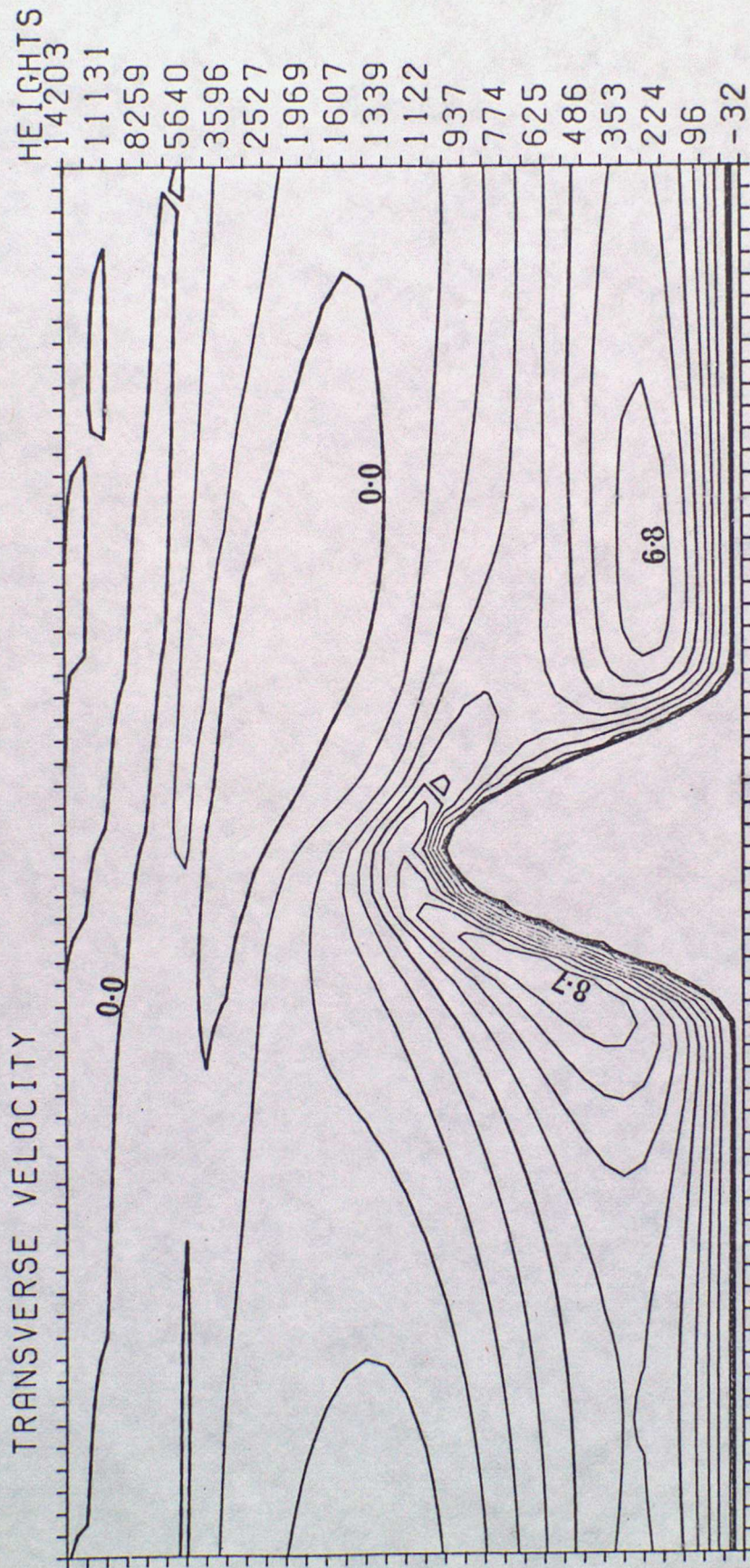


Fig 6 b...

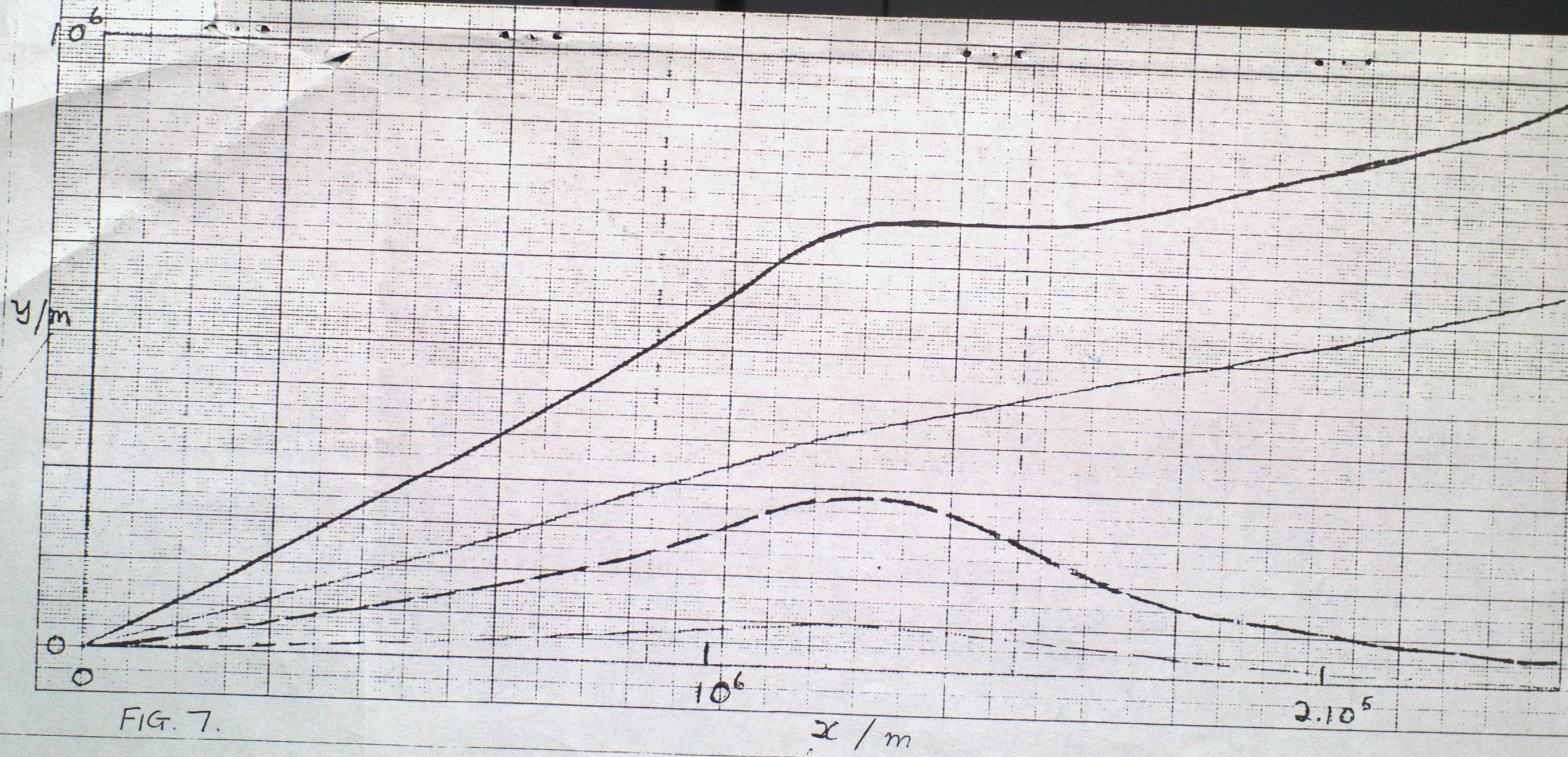


FIG. 7.